Journal of ELECTRONIC MATERIALS, Vol. 45, No. 6, 2016
DOI: 10.1007/s11664-016-4343-6
© 2016 The Minerals, Metals & Materials Society

CrossMark

Microstructural Evolution of SAC305 Solder Joints in Wafer Level Chip-Scale Packaging (WLCSP) with Continuous and Interrupted Accelerated Thermal Cycling

QUAN ZHOU,[1] BITE ZHOU,[1] TAE-KYU LEE,[2,3] and THOMAS BIELER[1,4]

1.—Chemical Engineering and Materials Science, Michigan State University, East Lansing, USA. 2.—Cisco Systems, Inc., San Jose, CA, USA. 3.—Mechanical and Materials Engineering, Portland State University, Portland, OR, USA. 4.—e-mail: bieler@egr.msu.edu

Four high-strain design wafer level chip scale packages were given accelerated thermal cycling with a 10°C/min ramp rate and 10 min hold times between 0°C and 100°C to examine the effects of continuous and interrupted thermal cycling on the number of cycles to failure. The interruptions given two of the samples were the result of periodic examinations using electron backscattered pattern mapping, leading to room temperature aging of 30 days–2.5 years after increments of about 100 cycles at several stages of the cycling history. The continuous thermal cycling resulted in solder joints with a much larger degree of recrystallization, whereas the interrupted thermal cycling tests led to much less recrystallization, which was more localized near the package side, and the crack was more localized near the interface and had less branching. The failure mode for both conditions was still the same, with cracks nucleating along the high angle grain boundaries formed during recrystallization. In conditions where there were few recrystallized grains, recovery led to formation of subgrains that strengthened the solder, and the higher strength led to a larger driving force for crack growth through the solder, leading to failure after less than half of the cycles in the continuous accelerated thermal cycling condition. This work shows that there is a critical point where sufficient strain energy accumulation will trigger recrystallization, but this point depends on the rate of strain accumulation in each cycle and various recovery processes, which further depends on local crystal orientations, stress state evolution, and specific activated slip and twinning systems.

Key words: Accelerated thermal cycling, lead-free solder, electron backscattered diffraction mapping, recrystallization, recovery, slip systems, twinning, crack nucleation, crack growth

INTRODUCTION

Accelerated thermal cycling is a common way to assess the reliability of electronic interconnects under thermo-mechanical cycling. Several studies have been carried out to compare accelerated testing and failure modes with real cases.[1–10] These studies focused on effects of temperature difference between dwell temperatures, holding time at dwell temperatures, time-weighted mean temperature, and ramp rate between dwell temperatures. However, there have not been introductions of long relaxation times during such tests in the studies reported to date, which differs from the relaxation that is very likely to happen in normal service applications when the electronic device may be running in a steady state condition for long periods of time, or shut down. Nevertheless, because microstructural evolution and damage evolution

(Received August 15, 2015; accepted January 9, 2016; published online February 2, 2016)

will be unique to each solder joint due to predominant grain orientation and position in the package regardless of test conditions, observations of a number of joints with both continuous and interrupted thermal cycling tests will provide valuable comparisons to elucidate failure mechanisms as a result of contrasting thermal cycling histories.

It has been widely reported in the literature that the primary failure mode in tin-based solder interconnects during accelerated thermal cycling is cracking in the bulk solder near the package side caused by the package/board coefficient of thermal expansion (CTE) mismatch.[9–15] Strain concentrations near the package side during thermal cycling triggers recrystallization, which creates high angle grain boundaries that are vulnerable to crack nucleation and propagation.[9–22] Tin-based solders usually contain one or only a few orientations with preferred boundaries after solidification.[1,11,12,16–18,23–25] This behavior amplifies the effects of the elastic, plastic, and CTE anisotropy of β-Sn,[1,11,13,15,17,26–28] leading to unique responses of each solder joint upon thermal cycling. Thus, it is necessary to evaluate the microstructural evolution in *individual* solder joints in packages having different dominant orientations and strain histories by analyzing how their thermal history affects the underlying thermal fatigue mechanisms leading to damage. In prior studies,[14,17,18,24,27,29–32] slip activity has been correlated with recrystallization and crack propagation to explain the microstructural change with different dominant crystal orientations and different stress/strain conditions during thermal cycling. In Ref. 32, a detailed quantitative study was performed following the thermal cycling histories of 20 SAC305 solder joints at certain intervals in a WLCSP configuration. Slip systems with higher Schmid factors were responsible for the observed microstructural changes, and in one instance, a particular slip system was directly related to a continuous recrystallization process that preceded the crack propagation within the same solder joint.

The thermal cycling history of the solder joints in Ref. 32 had significant differences from a typical accelerated thermal cycling test, where one or several package/printed circuit board (PCB) units are thermally cycled in a testing chamber until failure occurs. The samples in Ref. 32 had periods of ambient temperature storage (0.6 T_m) from 600 h to 2 years. These samples were initially sectioned, polished along the edge row, and characterized using orientation imaging microscopy™ (OIM). As these samples were part of a parallel effort using synchrotron x-ray characterization, there were periods of storage between periods of accelerated thermal cycling, so relaxation took place in ways not experienced in typical accelerated thermal cycling tests. This situation created a special case of mixed accelerated thermal cycling and room temperature aging for these high-strain WLCSP samples. In the present paper, analysis of microstructural evolution under

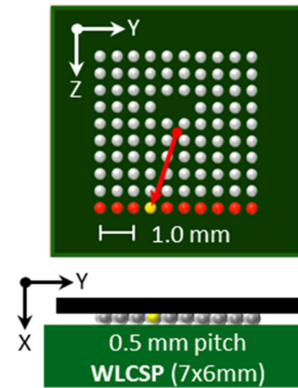

Fig. 1. Schematic of the plan view and a representative cross-section of a WLCSP; the red arrow illustrates the macroshear stress direction imposed on joint 4 by the CTE mismatch.

interrupted conditions will be compared with two samples with the same package design that were continuously thermally cycled to failure.[22] From analysis of these two conditions, the role of recrystallization on crack nucleation and growth will be elucidated.

EXPERIMENTAL PROCEDURES

Four wafer-level chip-scale package (WLCSP) samples were used in this study. The 7 × 6 mm WLCSP design has a 10 × 10 array of 250 μm diameter SAC305 solder balls with 0.5 mm pitch attached to a 2.4-mm-thick FR4 printed circuit board (PCB) (Fig. 1). The chip-side of the solder joint had a Ni/Au surface finish, and the board side had an organic surface protection (OSP) surface finish on Cu; more details are provided in Refs. 22, 31, and 32. Of these four units, two as-assembled samples (named A and B in Refs. 31 and 32) were pre-cross sectioned along the edge row without mounting, and they were assessed after different numbers of 0–100°C thermal cycles (TCs) with 10 min ramp rate and hold times after various room temperature hold times. The other two samples were from a large population that was continuously thermal cycled until the last package in the population failed (the as-assembled sample (C) was given 1625 cycles, and the 500 h 150°C pre-aged sample (D) was given 1110 TCs; Weibull plots and additional details are in Ref. 22).

Samples A and B were examined prior to thermal cycling using optical microscopy and electron backscattered diffraction (EBSD) to identify the initial microstructure. The thermal cycling and room temperature storage time history are shown in Fig. 2. This history was imposed by scheduling of synchrotron beam time for a parallel study of samples without any cross sectioning, the subject of a future paper. Observations following thermal cycling on cross sectioned samples were made with optical microscopes and a CamScan (Cambridge, UK) field emission scanning electron microscope (SEM) with OIM Data Collection (version 4.5) used for EBSD

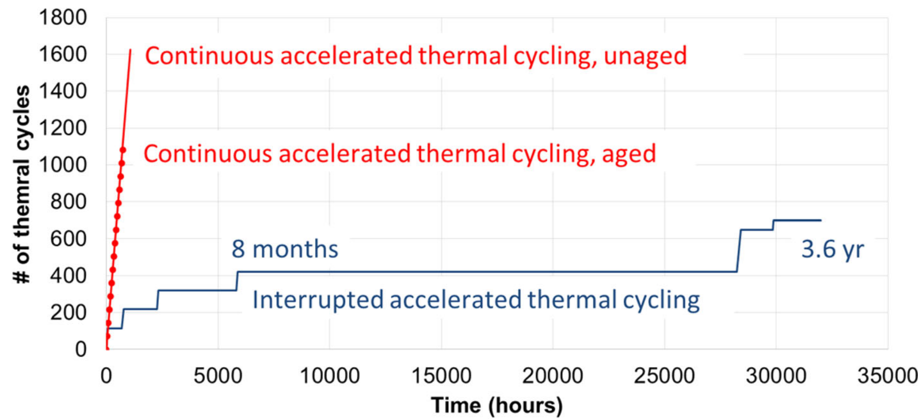

Fig. 2. History of continuous and interrupted accelerated thermal cycling.

analysis. Carbon paint was used to provide a conductive coating on the board and package, and in some locations, the paint covered some of the interfacial regions. EBSD data were further analyzed using OIM Analysis Software (version 5.1). "Neighbor confidence index correlation" and "Grain dilation" algorithms were used to clean-up (change pixels with low confidence or very small orientations, which arise mostly from grain boundaries or intermetallic particles). Most scans were cropped to remove areas of very low pattern image quality. After optical and SEM topographic characterization following 420 cycles, Samples A and B were lightly re-polished to remove the excessive oxide and surface features after optical characterization to improve EBSD measurements (and similarly for Sample A after 700 cycles). Because of the correlation between the *c* axis and the CTE anisotropy, *c* axis maps indicate how the normal stress component from the board varies during thermal cycling (so similar colors do not imply similar crystal orientations). At high temperature, joints with the *c* axis parallel to the interface (red/orange orientations) cause joints to be in tension, and when the *c* axis is perpendicular to the interface (purple/blue orientations) the joints are in compression.[18] In contrast, samples C and D were cross-sectioned after thermal cycling to failure along the edge row. Similar EBSD and OIM analysis was performed to obtain comparable data for both the continuous and interrupted pre-cross sectioned samples.

Slip trace analysis was done using optical and SEM images with OIM data using the methods described in Ref. 32. Euler angles are defined with X down and Y to the right. Estimates of the shear stress operating on the joint were obtained by assuming operation of a perfect shear stress radially from the center of the package. For example, in ball 4 illustrated in Fig. 1, a positive pure shear in the XY plane was rotated +108° from the Y direction about the X axis, which is representative of the shear stress arising from heating the sample (the board expands more than the package).

RESULTS

Microstructure Evolution During Continuous Thermal Cycling

Optical micrographs and *c* axis orientation maps from the post-test cross sectioned outer rows of samples C and D are shown in Fig. 3, which are the samples that failed at the characteristic life cycle number of TCs in the Weibull distribution.[22] All of the solder joints show new orientations near the package side that are different from the orientation in the center of the joint, indicating recrystallization. Some joints also show new orientations in the center, notably in joints that were initially solidification twinned, see arrows in joints 3 and 5 in sample C, and also in joints 6, 7, and 8 in sample D. * Recystallization occurred not only near the package side region but also along the board side and in the solder bulk, implying that the process driving recrystallization was active across the whole solder joint, not only near the package interface region. In the unaged joints, crack paths are much more tortuous than the aged joints, and 24% more cycles were required to cause failure than the aged joints. Pre-aging of Sn-Ag-Cu solder joints apparently facilitated recrystallization driven crack growth. The cracks in aged joints show less branching than in the not aged samples (Fig. 4). While only half of the aged joints had a crack all the way across the joint, aging led to more rapid crack growth in joints where recrystallization was more extensive.

Microstructure Evolution During Interrupted Thermal Cycling

Microstructure evolution and effects of slip activity resulting from the CTE mismatch in samples A and B are shown in the *c* axis maps in Fig. 5 up to 700 TCs. Each sample shows an outer row consisting of similar *c* axis orientations (almost parallel to

*There are also obvious artifacts of near-horizontal scratches that induced twins in joints 6, 8 in Sample C, and joints 3, 4 in Sample D.

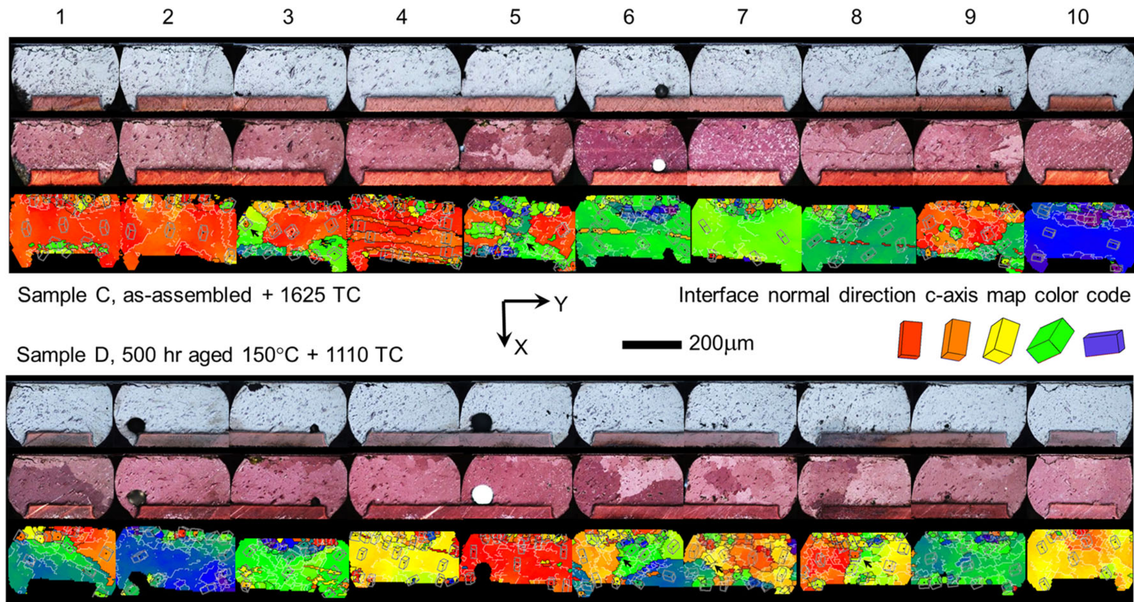

Fig. 3. Optical, polarized light, and *c* axis orientation maps of the outer row of solder joints from samples C and D, which failed at the characteristic times of 1373 and 1042 cycles, respectively. These samples were cycled until the last package in the population failed, at 1625 and 1110 cycles, respectively.

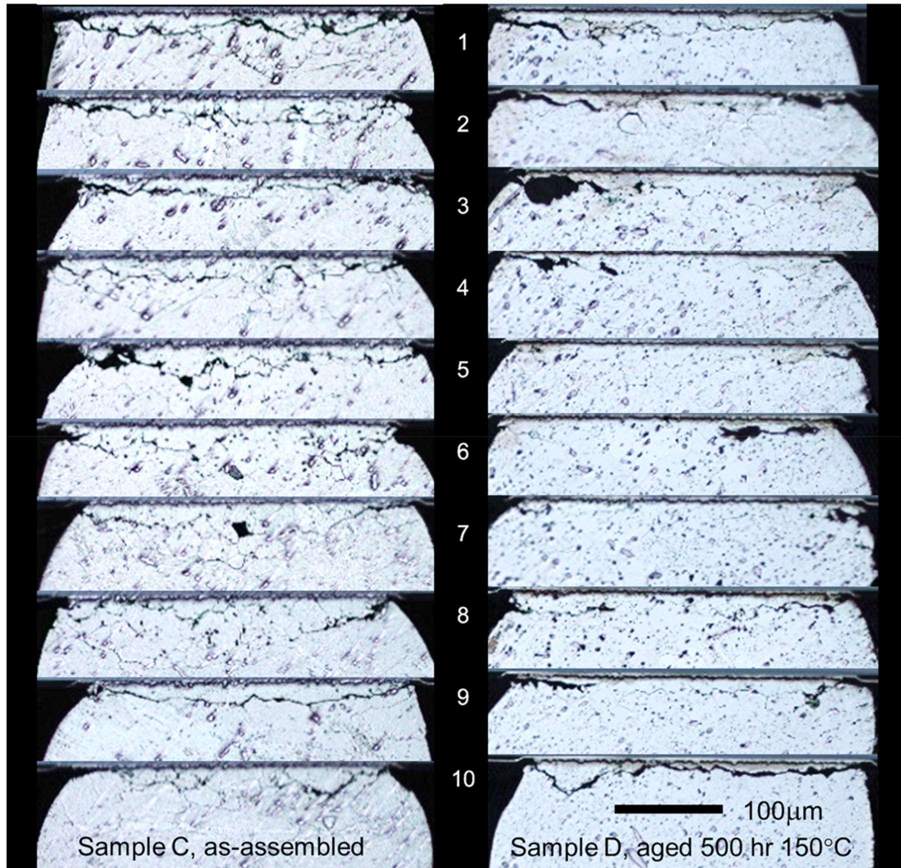

Fig. 4. Enlarged optical micrographs of cracks in continuous thermally cycled WLCSP packages illustrating crack paths.

the board in sample A, and inclined to the board in sample B) and all but one are apparently single crystals in the as-fabricated condition. Prior characterization of the deformation process up to 320 TCs indicated that the activity of slip systems with high Schmid factors accounted for the

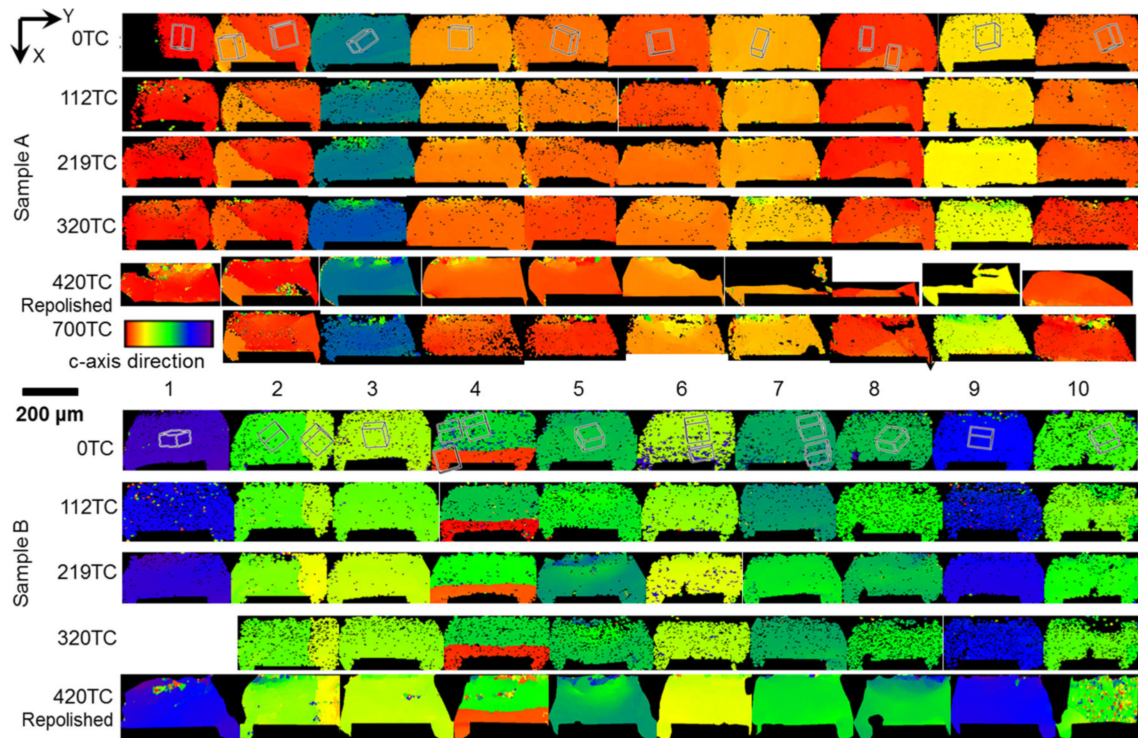

Fig. 5. *C* axis EBSD orientation maps of solder joints in pre-cross sectioned sample A and sample B at different thermal cycles. (The top of balls 6–10 in sample A at 420 TC was covered by carbon paint).

continuous recrystallization process (recovery to form low angle grain boundaries).[32] Also, while the two samples appear to have different highly preferred orientations, their crystal orientations vary more than it appears because the *c* axis map is not sufficient to reveal the crystal orientations; hence, crystal orientations are shown with prisms for the 0 TC samples. The *c* axis maps are important to show variations in CTE anisotropy, and they also correlate with differences in predominant slip activity. After 420 cycles, the quality of OIM imaging was poor, so after recording surface topography shown in Fig. 6, the samples were repolished to obtain good EBSD measurements. After aging for 2.5 years, they were then given 250 cycles in two stages (Fig. 2). The surface topography after 700 cycles was qualitatively similar to the deformation topography observed earlier for each joint. As the OIM quality after 700 cycles was again poor due to oxidation and topography, Sample A was lightly repolished again before making the maps shown in Fig. 5, and they are similar to prior maps. Figure 5 clearly shows *c* axis orientations that differ from the parent *c* axis orientation in all joints in sample A, and for joints 1, 4, 5 and 8 in sample B.

Secondary electron images of sample A after 700 TCs in Fig. 7 show the crack morphology more clearly than optical micrographs in Fig. 6 (though the optical micrographs show the slip traces more clearly). The slip traces near the package side in Fig. 6 indicate that during the last increment of 250 TCs, there was some active slip deformation in most of the joints, but grain boundary sliding of recrystallized grains is more easily seen. The dark areas in optical micrographs are grains with surfaces that are tilted from the surface normal and do not reflect light back into the lens. Some recrystallization/grain boundary sliding features can also be observed near the *board side* of the solder joints in joints 1, 2, 4, 9, and 10 in Fig. 6 (bottom of the solder joints), but there was no evidence of a crack near the board side. The recrystallized areas near the package side showed significant topographic features, suggesting that the recrystallized grains were pushed out or rotated near the interface.

Sample A had more obvious deformation features than sample B, and the damage mode in the two samples indicated that small amounts of recrystallization promoted crack propagation along the newly formed random high angle grain boundaries in the solder bulk near the package side. Comparing the microstructure change in samples A, B with C, D clearly shows how interrupted thermal cycling leads to much smaller regions of recrystallization, in contrast to well-established recrystallized regions resulting from continuous thermal cycling. More than 1000 cycles were needed to form a similar degree of cracking in all of the interrupted thermal cycling joints that were apparent after 700 uninterrupted TCs (Figs. 4 and 7).

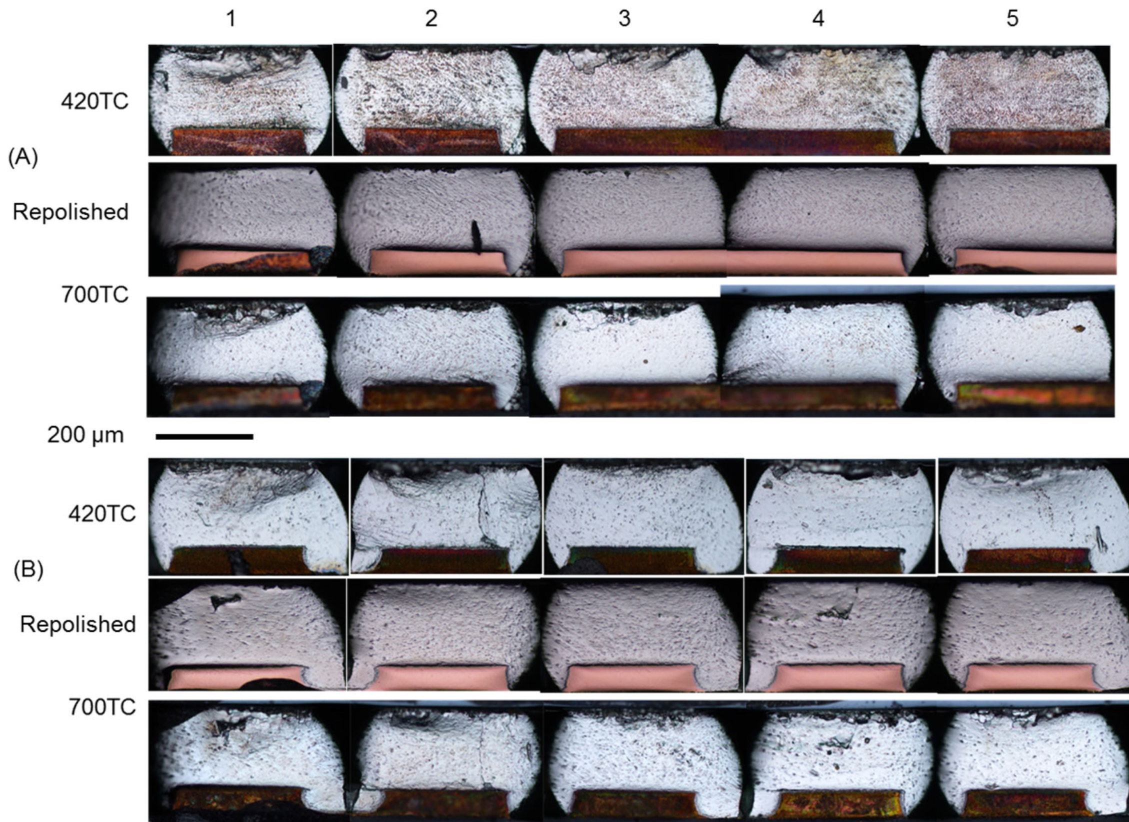

Fig. 6. Optical micrographs of joints 1–5 in samples A and B after 420 thermal cycles, showing topographic effects of slip activity concentrated near the package side. The samples were repolished for OIM measurement, and then given another 250 cycles, and similar topographic features developed.

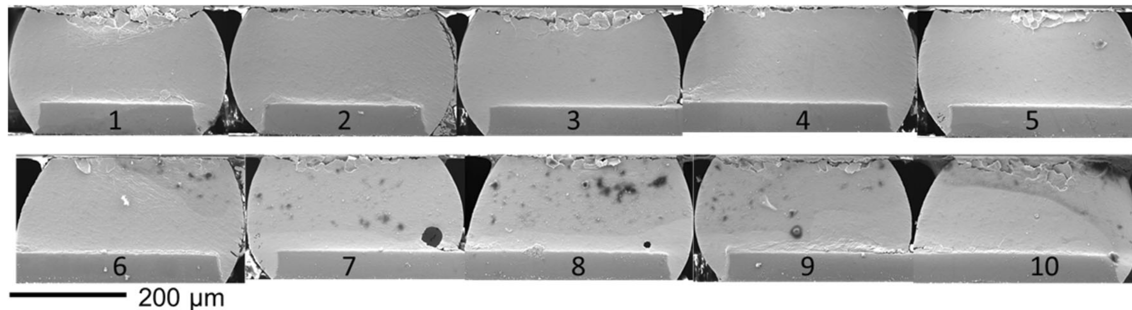

Fig. 7. Secondary electron images of solder joints in sample A after 700 thermal cycles (sample was re-polished after 420 TC).

The slip activity prior to cracking with minimal recrystallization is examined in more detail for ball 4 of Sample A in Figs. 8, 9, and 10, using the same analysis strategy used in Ref. 32. Distinct slip traces (red arrow) were evident after 112 cycles associated with a commonly observed (110)[001] slip system with a modest Schmid factor of 0.4 (see magenta slip trace and unit cell above the images). These two slip bands are correlated with a low angle boundary (indicated by white lines on the *c* axis orientation map) that was not initially present. The low angle boundary is parallel to the slip bands, and the estimated misorientation angle and axis is noted below the OIM map, showing that the rotation axis was close to [100];** this is not the rotation axis expected for slip on the (110)[001] system. Rather, the highest Schmid factor slip system with m = 0.64 on the (011)$[01\bar{1}]$ has a rotation axis of [100], and

**Multiple misorientation measurements between pixels yield similar misorientations that reflect a variety of different symmetric crystal orientations, so the reported angle/axis is a representation of the trend. Also, as the rotation axis is expressed in Cartesian coordinates, the z component of the rotation axis is multiplied by c/a = 0.5456, to make the reported rotation axis crystallographically meaningful for the Sn unit cell.

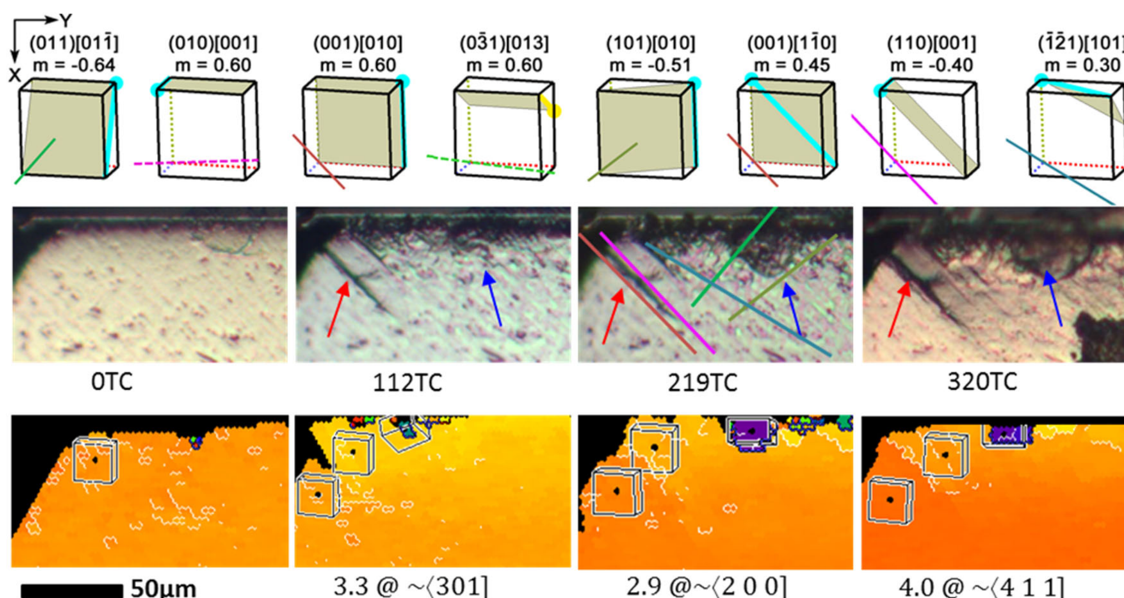

Fig. 8. Optical micrographs illustrating slip system traces (with correlated slip system identification) and OIM maps showing recrystallization in Sample A ball four with an initial orientation of φ_1, Φ, φ_2 = 44°, 23°, 45°, at different stages of thermal cycling (TC). Thick black boundaries are high angle, thin white are low angle. Not shown are slip systems with high Schmid factors with no observed slip traces: (10$\bar{1}$)[010] m = 0.55, and (011)[1$\bar{1}$1] m = 0.51.

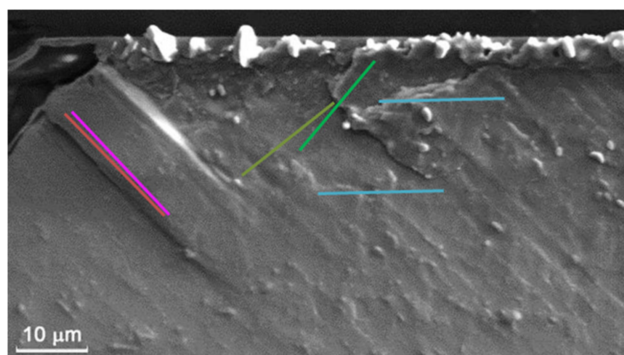

Fig. 9. Secondary electron image of the upper left corner of Sample A ball 4 after 219 thermal cycles prior to repolishing.

faint slip traces are evident for this system.[†] Slip traces on three other systems with high Schmid factors were also observed after 219 cycles (see colored traces near the blue arrows, and illustrations of these slip systems above the maps). Figure 9 provides detail of the slip band topography, showing an inclined flat surface consistent with the (110)[001] slip system along the most obvious slip band; notably, these large slip bands did not continue to grow after 112 TC.

After 112 cycles, some small recrystallized grains are evident, but these particular orientations were not observed after 219 cycles, and instead a different (purple orientation) in the same region appeared, and it remained stable, as it was also evident after 320 cycles. There are also very irregular small extrusions or whisker features along the interface in Fig. 9 that may account for scattered small orientation measurements along the interface.

To minimize the influence of the small interface topographic features, fine scans were made by rotating the sample 90° about the polished surface normal, so that these small topographic features would interfere less while measuring the grain orientations near the interface. These finer scans revealed more detail about the grains surrounding the purple grain, as illustrated in Fig. 10 (black areas are regions of very low pattern image quality that were cropped out in the 219 cycle map). Above the purple grain, there is a light green grain (φ_1, Φ, φ_2 = 69°, 30°, 17°, close to the parent orange grain orientation φ_1, Φ, φ_2 = 44°, 23°, 45°), which is rotated slightly about the z crystal axis, and more about the x axis, consistent with operation of the highly stressed (011)[01$\bar{1}$] slip system with $m = -0.69$ (the negative Schmid factor implies that the sense of shear was up on the visible surface of the slip plane). The Schmid factor for this green orientation is higher than the 0.64 parent orange orientation value. The prisms to the left of the map also show a (0$\bar{3}$1)[013] mechanical twin system (the slip plane is nearly invisible, due to being perpendicular to the page). The purple orientation is a mechanical twin of the light green orientation, evident by the 58° rotation about a (nearly) common horizontal $\langle a\rangle$ axis. Within the purple twin, two

[†]It is likely that slip traces are faint because the slip plane is nearly parallel to the surface—this is also indicated by shorter plane traces on the prisms.

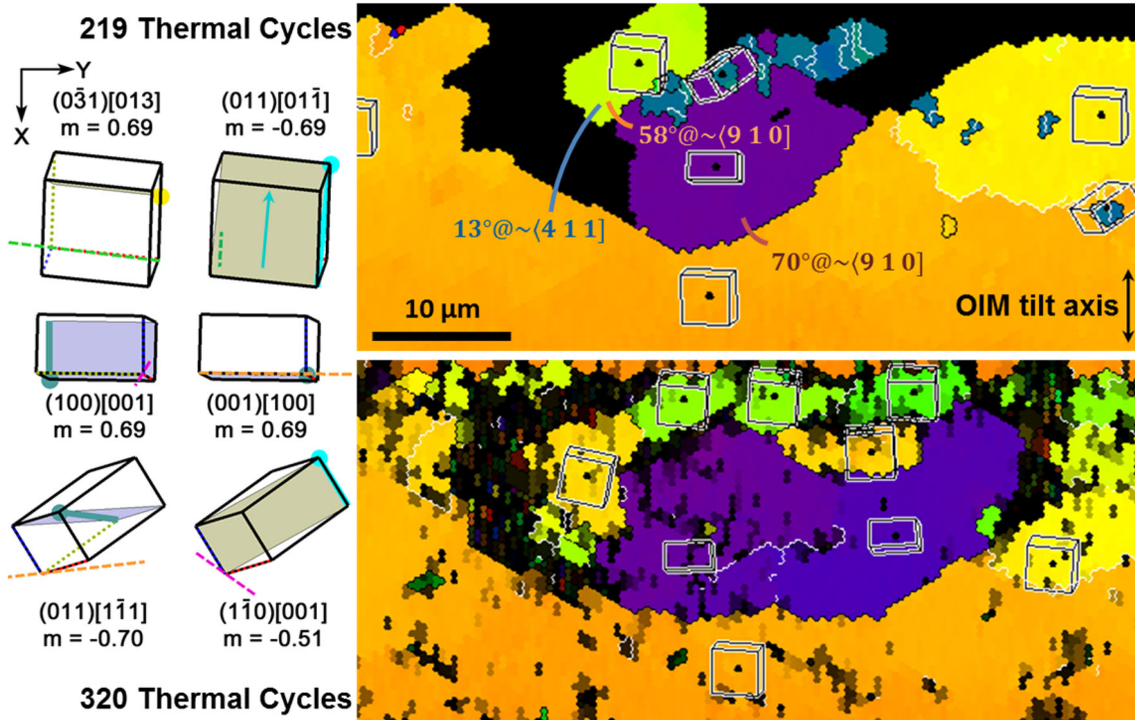

Fig. 10. Examination of recrystallized grain, which probably formed by mechanical twinning in Sample A ball 4. Low angle boundaries are white and high angle boundaries are black. The 320 cycle map has a confidence index overlaid, to darken low confidence pixels.

highly stressed slip systems are illustrated. The other blue orientation in the midst of the twin is also found in other nearby regions, which is highly misoriented from the parent orientation, and is probably a recrystallized grain; two highly stressed and facile slip systems are illustrated. After 320 TCs, the same region showed that the twinned region grew, and the parent green orientation was indexed more effectively, but the blue orientation that was observed earlier disappeared. Due to increased surface topography and oxidation, this map has many more low confidence index pixels indicated by an overlaid gray to black scale to identify regions of confidence index below 0.1.

DISCUSSION

From this study as well as others,[9,10] it is not completely obvious if recrystallization is the cause of crack propagation, as cracks also propagated in regions that were not recrystallized. Continuously cycled samples C and D sustained more TCs before failure, and they had more recrystallization and less recovery, which seems to contradict recrystallization driven cracking as a fast failure process—it may actually be a slower failure process than when recovery was prevalent. This suggests that crack growth may be more driven by time under load than by microstructure evolution. Because failure occurred within the solder typically along high-angle grain boundaries, and not at the intermetallic interface, the evolution of the solder/metallization at the interface is probably not directly important to the failure mechanism. These issues can be examined in this work because most of the prior studies did not use sequential observations on pre-cross sectioned samples. Observations made from freshly polished cracked surfaces near the package side of the joint lack information about history. Also, the packages used in most prior studies were low-strain designs, in which strain accumulation per cycle was much lower so that recrystallization was not as extensive as in the present study.

Competition Between Recrystallization and Recovery

During thermal cycling, strain energy is accumulated in the form of defects in the solder joint from each cycle. Since the lower dwell temperature is above 0.5 T_m (−28°C), recovery and recrystallization mechanisms are active during thermal cycling and room temperature storage (25°C). Recovery is defined as various processes (e.g., vacancy annihilation, dislocation climb-annihilation, reorganization to form low angle boundaries) that release the stored energy in deformed materials without the migration of high angle grain boundaries, whereas recrystallization is the formation of new grains in deformed materials by means of formation and migration of high angle grain boundaries driven by the stored defect energy.[33] With each cycle, partial relaxation of the stress occurs due to recovery processes where some of the dislocations that moved under the imposed loading disappear. With a reverse in temperature, many of the non-recovered

dislocations could move in the reverse direction unless recovery led to forming locks or jogs that impede reverse flow (discussed further below). With each cycle, some dislocations are absorbed into subgrain boundaries, increasing the misorientation slightly. Because more recovery of dislocation occurs at high temperature than at low temperature, thermal cycling leads to asymmetric recovery processes, so more dislocation accumulation takes place during the cooling and cold part of the cycle.

Recovery and recrystallization are two competing processes in a thermal cycled solder joint. Due to the lower activation barrier for recovery,[14] stored strain energy from each TC will be constantly released through the recovery process. There is enough time for recovery to take place, this reduces the driving force for recrystallization. Thus, continuous thermal cycling will cause more accumulation of strain energy, and in the high strain design of the WLCSP package, this can occur at a rate faster than its release by recovery,[9] leading to conditions that favor formation of a recrystallization nucleus.

In the continuous thermal cycling condition (samples C and sample D), the *c* axis maps in Fig. 3 show much more orientation (color) gradients than the interrupted samples, implying that accumulated dislocations during each cycle led to orientation changes. Strain-concentrated regions near the package side enabled recrystallization after an incubation period,[9–12,15,20,21,28] and nominally 30 μm recrystallized orientations covering most of the interface region developed. In some orientations, recrystallized orientations also developed in the center of the joint.

Both continuous and discontinuous recrystallization resulted. Continuous recrystallization developed by dislocation rearrangement to form low angle grain boundaries (white lines in Fig. 3), with misorientations that increased gradually with strain cycles, and in some places, became mobile high angle boundaries. Discontinuous recrystallization also occurred in larger strain regions, where significantly different orientations from the parent orientation emerged after an incubation time. As high angle grain boundaries have lower cohesive energy, they can slide, leading to incompatibilities that facilitate crack opening. With accumulated defect storage from deformation through further thermal cycling, both recrystallization processes spread toward the center of the solder joint as described in Ref. 31.

The lesser amount of recrystallization in the interrupted accelerated thermal cycling can be attributed to the long room temperature hold (aging) times. This is the only difference between the two tests (assuming that the free surface in the pre-cross sectioned sample did not significantly affect recovery and recrystallization processes). Clearly, the volume of orientation change from recrystallization is much smaller, with smaller grain sizes in Fig. 5 than in the continuously cycled joints in Fig. 3. In the interrupted thermal cycled samples A and B, there are scattered recrystallized grains with 10–20 μm grain sizes, and they typically do not dominate the interfacial region. While interrupted samples show evidence of recrystallization related cracking near the package side,[32] Fig. 5 shows that the bulk orientation of all the solder joints (including several bi-crystals) did not change very much between each set of TCs. This implies that there is little change in grain orientation (and hence, little accumulated dislocation activity). Thus, 100 accelerated TCs barely provided sufficient accumulated strain energy to nucleate recrystallized grains near the most highly strained interface, but dislocation recovery during the hold time was substantial, which robbed the material of a driving force for growth of the rare recrystallized nuclei.

The time for stress relaxation at room temperature converts elastic strain energy into plastic strain and reduces the internal stress; hence, interruption leads to more plastic strain, and subsequent removal of dislocations by recovery. The effect of internal elastic strain is illustrated by Choi et al.[34] who showed that after thermal cycling and 10 months of room temperature storage, surface topographic features on a polished surface developed due to ledge formation resulting from grain boundary sliding. Topographic features resulting from strain accumulation also developed *during* thermal cycling, as evident in sequential images in Fig. 8. In the continuously cycled high-strain package design joints C and D used in this study, the optical images shown in Fig. 4 were taken 2 years after the sample was initially polished, so the lack of topography implies that internal stresses were relaxed due to the crack (i.e., due to relaxation that occurred prior to preparing the polished surface).

After 700 cycles, Fig. 7 shows evidence of faint slip traces similar to those observed prior to 420 cycles. This suggests that the driving force for slip must have decreased as the crack grew across the joint. While no cracks were obvious after 420 cycles, the fact that 250 cycles led to complete cracking following a long recovery period of about 2 years implies that the presence of small recrystallized grains facilitated crack propagation in the regions where they existed during the 250 cycle period. Despite the difference in the amount of recrystallization, the failure mode under the two different thermal cycling conditions was similar; crack propagation along the high angle grain boundaries that formed after recrystallization. The magnitude of recrystallization in the interrupted samples A and B was much less extensive and, thus, more concentrated near the interface, so the crack followed much closer to the interface. The presence of small recrystallized grains, and their stability with long hold times is important, and this is examined in more detail in the focused analysis presented in Figs. 8, 9, and 10.

Stability of Recrystallized Grains

A steady generation of dislocations in the parent orientation(s) provide a driving force for forming a recrystallized grain nucleus, which may or may not survive. Figure 10 provides two contrasting cases: the slightly rotated (green) parent grain is misoriented from the parent grain by a 13° low angle boundary, and it has higher Schmid factors for the slip systems that were active. This more stable orientation led to a more favorable condition for $(011)[01\bar{1}]$ slip, and also to form a mechanical twin, as the rotation increased both Schmid factors to 0.69. The purple twinned orientation has high Schmid factors of 0.69 for two slip systems that are perpendicular to each other, (100)[001] and (001)[100]. The former is a more facile slip system than the latter, but both are needed to accomplish the shear. Thus, these two complimentary shears needed to accomplish pure shear could be limited by the less facile system, which could result in less deformation (and fewer dislocations implies a lesser driving force for recovery or recrystallization). Blue/purple orientations are known to be more resistant to the continuous recrystallization process.[22,32] This orientation also has a large CTE mismatch with the neighboring orange grain, which could cause high local stresses and localized slip in the softer of the two grain orientations. As the purple twin grain probably deformed less than the surrounding green and orange orientations, more dislocations would be expected in the grains surrounding the twin, giving it the twin a growth advantage that is observed in Fig. 10.

In contrast to the stable twin orientation, after 119 TC, several small recrystallized orientations disappeared. The blue orientation in Fig. 10 that formed after 219 cycles[‡] also disappeared prior to 320 TC. This is a soft orientation in which many dislocations can be generated; it had high Schmid factors for facile $\langle 111 \rangle$ and $\langle 001 \rangle$ slip directions and several subgrain boundaries are evident in these orientations. Such a grain could have more dislocation content than the surrounding orange or purple grains, and its higher defect energy could favor its disappearance due to grain boundary migration of the larger parent grain or twin neighbors that consumed them.

Strengthening Due to Recovery

During the hold times of at least 600 h, most of the stored elastic strain energy was released before the next round of TCs, which led to a recovered dislocation substructure. Figure 8 illustrates how regions where slip was active before could be halted by formation of a low angle boundary. Here, a dramatic slip band ledge formed during the first 100 cycles. This ledge formed by a facile (110)[001] slip system that had a modest Schmid factor of 0.4. The (011)[011] slip system with the highest Schmid factor of 0.64 is also known to be active, but because its slip vector is nearly parallel to the surface, it was not as obvious as the more facile system. After the first 112 cycles, it is likely that the subgrain boundaries that formed included dislocations from both slip systems, and locked up the [001] dislocations on the more facile but less favored system. Thus, the interruption led to a recovery process that altered the dislocation substructure to prevent subsequent activation of a facile slip system, which hardened the crystal. The conditions that favor recrystallization were halted locally, as defect generation was halted. As the recovery enabling interruption was repeated three times, accumulation of strain energy that could drive recrystallization was reduced due to the hardening presence of subgrain boundaries; instead, recrystallization could only be active in the most highly strained region near the package interface. Hence, the relaxation in samples A and B after each interval of thermal cycling led to a recovery dominated microstructure evolution mechanism.

Recovery Versus Recrystallization Effects on Crack Growth

As evident in comparing Fig. 4 with Fig. 7, the interrupted sample cracked much closer to the interface, where the much fewer number of recrystallized grains were located. Hence, the crack length is shorter and less tortuous, so that fewer cycles were necessary to percolate the crack through the joint. Less recrystallization and more established subgrain boundaries increased the hardness, which led to a higher elastic driving force for crack growth through the unrecrystallized material. This may also account for the observation in prior work[3] that longer dwell times at high temperatures led to a higher residual strength after cycling than dwell times at low temperature, where recovery processes would be slower. Also, slower heating and cooling rates would allow more recovery, and, consequently, less driving force for recrystallization.

In the above comparison, the driving force for recrystallization is diminished in the high-strain WLCSP package when there is a long relaxation between each ~100 TCs. If the intervals for relaxation were more frequent (i.e., every 30 cycles), it is reasonable to think that recrystallization would be even more suppressed. If recrystallization was completely suppressed by recovery, then there would be no high angle boundaries where cracks could nucleate, so crack nucleation would require a higher stress than a recrystallized microstructure.

[‡]This orientation appears as if it could be a twinned twin of the green tilted parent orientation, but this is unlikely because the blue orientation is clearly misoriented by ~20° from the possible twinned twin (and the Schmid factors for twins that could accomplish this are ranked ~25th of 56 slip and twin systems), so the origin of the blue Rx grains is unexplained.

Without crack nucleation, there can be no crack growth, leading to very long-term stability, such as that observed by Hokka et al.,[9,10] where no recrystallization occurred in samples with a thermal cycling history much like normal interior use conditions.

In contrast, where much recrystallization occurs, soft grains without subgrains and high angle (high energy) boundaries that slide develop, and this consequently leads to an increase in potential crack sites[4] that could also relax long range accumulated stress. The large number of grain boundaries makes the joint able to deform via both slip and grain boundary sliding, where more grain boundaries lead to a more compliant (and possibly damage *tolerant*) state.[35] The difference in the number of cycles to failure in the two continuous accelerated thermal tests with as-fabricated and aged microstructures can be explained by the coarsening of intermetallic particles and their decrease in quantity. With aging, it did not take as long to develop a recrystallized microstructure condition, because fewer and larger particles reduce the pinning effect on dislocations and grain boundaries while also stimulating recrystallization nuclei at the larger particles that accelerates recrystallization that enabled crack propagation along recrystallized grain boundaries.[9–11,13,18,19,28] In the as-fabricated condition, smaller and more closely spaced precipitates lead to smaller recrystallized grains, which would have a lesser degree of sliding incompatibility. The more homogeneous distribution of grain boundaries with less severe incompatibilities then resulted in a more gradual development of crack paths; Fig. 4 shows much more tortuous crack paths in the unaged sample.

In the interrupted accelerated cycling condition, recrystallized grains were smaller, less stable, and developed close to the interface. With periodic long recovery times, a hardened microstructure with stable subgrain boundaries developed, so elements of both types of microstructure developed with high angle grain boundaries that facilitated crack nucleation and a hardened subgrain microstructure. This combination led to a more vulnerable condition, where a higher residual stress led to fewer TCs needed to percolate the crack all the way across the joint.

This comparison shows that recrystallization is probably responsible for crack nucleation, but growth can be retarded by a network of boundaries that cause branching. Without a branching opportunity, and a higher elastic stress state in a stable recovered microstructure, a nucleated crack can grow through the bulk solder. Thus recrystallization is both a benefit and a problem, so managing the recovery and recrystallization processes strategically may lead to identification of an optimal balance of evolution processes that could maximize the joint lifetime.

CONCLUSION

Four high-strain WLCSP packages were tested in either continuous or interrupted thermal cycling experiments. Interrupted thermal cycling allowed the samples to stay at room temperature for at least 600 h between each ~100 TCs, and a stable and strong recovered microstructure developed. Continuous thermal cycling resulted in solder joints with a much larger degree of recrystallization and less recovery. Nonetheless, the failure mechanism for both conditions is the same, with cracks nucleating along high angle grain boundaries formed during recrystallization. Crack propagation depends on the microstructure the cracks move through, leading to three cases:

(1) Thermal cycling with modest thermal strains and long hold times results in recovery but no recrystallization; a stable subgrain microstructure develops, which strengthens the microstructure, but no mechanism for crack nucleation develops until a low angle boundary becomes high angled, and can slide.
(2) Interrupted accelerated thermal cycling leads to isolated recrystallized grains that provide nucleation sites for cracks in high angle boundaries, but the microstructure is dominated by a strengthened recovered microstructure, leading to high elastic stress states that can drive the crack through the bulk solder relatively quickly.
(3) Continuous accelerated thermal cycling imposes large strains stimulates recrystallization, and provides little opportunity for recovery, and the large strains at crack tips further stimulated recrystallization ahead of the crack. This leads to an extended network of high angle boundaries that can slide to facilitate stress relaxation, deflect crack propagation, and slow the rate of crack growth.

This work shows that there is a critical point where sufficient energy accumulation will trigger recrystallization, but this point depends on the rate of strain accumulation and recovery processes, which further depend on local crystal orientations, stress states evolution, and activated slip and twinning systems.

ACKNOWLEDGEMENTS

This work was supported by NSF-GOALI Award 1006656 and Cisco Systems Inc., San Jose, CA.

REFERENCES

1. P. Borgesen, T. Bieler, L.P. Lehman, and E.J. Cotts, *MRS Bull.* 32, 360 (2007).
2. J.G. Lee, L. Telang, K.N. Subramanian, and T.R. Bieler, *J. Electron. Mater.* 31, 1152 (2002).
3. J.G. Lee and K.N. Subramanian, *J. Electron. Mater.* 32, 523 (2003).
4. J.G. Lee and K.N. Subramanian, *Microelectron. Reliab.* 47, 118 (2007).

5. J.H.L. Pang, T.H. Low, B.S. Xiong, L.H. Xu, and C.C. Neo, *Thin Solid Films* 462, 370 (2004).
6. A. Syed and IEEE, In *54th Electronic Components & Technology Conference, Vols 1 and 2, Proceedings*, (IEEE: New York, 2004), p. 737.
7. S. Terashima, T. Kohno, A. Mizusawa, K. Arai, O. Okada, T. Wakabayashi, M. Tanaka, and K. Tatsumi, *J. Electron. Mater.* 38, 33 (2009).
8. T.T. Mattila, H. Xu, O. Ratia, M. Paulasto-Krockel, and IEEE, *2010 Proceedings 60th Electronic Components and Technology Conference (ECTC* 2010*)*, p. 581.
9. J. Hokka, T.T. Mattila, H.B. Xu, and M. Paulasto-Krockel, *J. Electron. Mater.* 42, 963 (2013).
10. J. Hokka, T.T. Mattila, H.B. Xu, and M. Paulasto-Krockel, *J. Electron. Mater.* 42, 1171 (2013).
11. D.W. Henderson, J.J. Woods, T.A. Gosselin, J. Bartelo, D.E. King, T.M. Korhonen, M.A. Korhonen, L.P. Lehman, S.K. Kang, P. Lauro, D.Y. Shih, C. Goldsmith, and K.J. Puttlitz, *J. Mater. Res.* 19, 1608 (2004).
12. S. Terashima, K. Takahama, M. Nozaki, and M. Tanaka, *Mater. Trans.* 45, 1383 (2004).
13. T.T. Mattila and J.K. Kivilahti, *J. Electron. Mater.* 35, 250 (2006).
14. A.U. Telang, T.R. Bieler, A. Zamiri, and F. Pourboghrat, *Acta Mater.* 55, 2265 (2007).
15. H.T. Chen, J. Han, J. Li, and M.Y. Li, *Microelectron. Reliab.* 52, 1112 (2012).
16. A.U. Telang, T.R. Bieler, J.P. Lucas, K.N. Subramanian, L.R. Lehman, Y. Xing, and E.J. Cotts, *J. Electron. Mater.* 33, 1412 (2004).
17. T.R. Bieler, H.R. Jiang, L.P. Lehman, T. Kirkpatrick, E.J. Cotts, and B. Nandagopal, *IEEE Trans. Compon. Packag. Technol.* 31, 370 (2008).
18. T.R. Bieler, B. Zhou, L. Blair, A. Zamiri, P. Darbandi, F. Pourboghrat, T.K. Lee, and K.C. Liu, *J. Electron. Mater.* 41, 283 (2012).
19. H.T. Chen, T. Mattila, J. Li, X.W. Liu, M.Y. Li, and J.K. Kivilahti, *Localized Recrystallization and Cracking Behavior of Lead-free Solder Interconnections under Thermal Cycling* (New York: IEEE, 2009).
20. T. Laurila, T. Mattila, V. Vuorinen, J. Karppinen, J. Li, M. Sippola, and J.K. Kivilahti, *Microelectron. Reliab.* 47, 1135 (2007).
21. J. Li, T.T. Mattila, and J.K. Kivilahti, *J. Electron. Mater.* 39, 77 (2010).
22. T.-K. Lee, B. Zhou, and T.R. Bieler, *IEEE Trans. Compon. Packag. Technol.* 2, 496 (2012).
23. R. Kinyanjui, L.P. Lehman, L. Zavalij, and E. Cotts, *J. Mater. Res.* 20, 2914 (2005).
24. A.U. Telang and T.R. Bieler, *JOM* 57, 44 (2005).
25. S.K. Seo, S. Kang, D.Y. Shih, and H. Lee, *J. Electron. Mater.* 38, 257 (2009).
26. K.N. Subramanian and J.G. Lee, *J. Mater. Sci.* 15, 235 (2004).
27. T.K. Lee, B.T. Zhou, L. Blair, K.C. Liu, and T.R. Bieler, *J. Electron. Mater.* 39, 2588 (2010).
28. L. Yin, L. Wentlent, L.L. Yang, B. Arfaei, A. Oasaimeh, and P. Borgesen, *J. Electron. Mater.* 41, 241 (2012).
29. B. Zhou, T.R. Bieler, T.K. Lee, and K.C. Liu, *J. Electron. Mater.* 39, 2669 (2010).
30. B. Zhou, G. Muralidharan, K. Kurumadalli, C.M. Parish, S. Leslie, and T.R. Bieler, *J. Electron. Mater.* 43, 57 (2014).
31. B. Zhou, T.R. Bieler, T.K. Lee, and W.J. Liu, *J. Electron. Mater.* 42, 319 (2013).
32. B. Zhou, Q. Zhou, T.R. Bieler, and T.K. Lee, *J. Electron. Mater.* 44, 895 (2015).
33. R.D. Doherty, D.A. Hughes, F.J. Humphreys, J.J. Jonas, D.J. Jensen, M.E. Kassner, W.E. King, T.R. McNelley, H.J. McQueen, and A.D. Rollett, *Mater. Sci. Eng., A* 238, 219 (1997).
34. S. Choi, K.N. Subramanian, J.P. Lucas, and T.R. Bieler, *J. Electron. Mater.* 29, 1249 (2000).
35. P. Darbandi, T.R. Bieler, F. Pourboghrat, and T.K. Lee, *J. Electron. Mater.* 43, 2521 (2014).